Measurement of the *CP* violating phase ϕ_s in $\overline{B}_s^0 \to J/\psi f_0(980)$

The LHCb Collaboration[1]

Abstract

Measurement of mixing-induced *CP* violation in $\overline{B}_s^0$ decays is of prime importance in probing new physics. So far only the channel $\overline{B}_s^0 \to J/\psi\phi$ has been used. Here we report on a measurement using an LHCb data sample of $0.41\,\mathrm{fb}^{-1}$, in the *CP* odd eigenstate $J/\psi f_0(980)$, where $f_0(980) \to \pi^+\pi^-$. A time dependent fit of the data with the $\overline{B}_s^0$ lifetime and the difference in widths of the heavy and light eigenstates constrained to the values obtained from $\overline{B}_s^0 \to J/\psi\phi$ yields a value of the *CP* violating phase of $-0.44 \pm 0.44 \pm 0.02$ rad, consistent with the Standard Model expectation.

---

[1]Authors are listed on the following pages.

The LHCb Collaboration

R. Aaij[23], C. Abellan Beteta[35,n], B. Adeva[36], M. Adinolfi[42], C. Adrover[6], A. Affolder[48],
Z. Ajaltouni[5], J. Albrecht[37], F. Alessio[37], M. Alexander[47], G. Alkhazov[29],
P. Alvarez Cartelle[36], A.A. Alves Jr[22], S. Amato[2], Y. Amhis[38], J. Anderson[39],
R.B. Appleby[50], O. Aquines Gutierrez[10], F. Archilli[18,37], L. Arrabito[53], A. Artamonov [34],
M. Artuso[52,37], E. Aslanides[6], G. Auriemma[22,m], S. Bachmann[11], J.J. Back[44],
D.S. Bailey[50], V. Balagura[30,37], W. Baldini[16], R.J. Barlow[50], C. Barschel[37], S. Barsuk[7],
W. Barter[43], A. Bates[47], C. Bauer[10], Th. Bauer[23], A. Bay[38], I. Bediaga[1], S. Belogurov[30],
K. Belous[34], I. Belyaev[30,37], E. Ben-Haim[8], M. Benayoun[8], G. Bencivenni[18], S. Benson[46],
J. Benton[42], R. Bernet[39], M.-O. Bettler[17], M. van Beuzekom[23], A. Bien[11], S. Bifani[12],
T. Bird[50], A. Bizzeti[17,h], P.M. Bjørnstad[50], T. Blake[37], F. Blanc[38], C. Blanks[49],
J. Blouw[11], S. Blusk[52], A. Bobrov[33], V. Bocci[22], A. Bondar[33], N. Bondar[29],
W. Bonivento[15], S. Borghi[47,50], A. Borgia[52], T.J.V. Bowcock[48], C. Bozzi[16],
T. Brambach[9], J. van den Brand[24], J. Bressieux[38], D. Brett[50], M. Britsch[10],
T. Britton[52], N.H. Brook[42], H. Brown[48], A. Büchler-Germann[39], I. Burducea[28],
A. Bursche[39], J. Buytaert[37], S. Cadeddu[15], O. Callot[7], M. Calvi[20,j], M. Calvo Gomez[35,n],
A. Camboni[35], P. Campana[18,37], A. Carbone[14], G. Carboni[21,k], R. Cardinale[19,i,37],
A. Cardini[15], L. Carson[49], K. Carvalho Akiba[2], G. Casse[48], M. Cattaneo[37], Ch. Cauet[9],
M. Charles[51], Ph. Charpentier[37], N. Chiapolini[39], K. Ciba[37], X. Cid Vidal[36],
G. Ciezarek[49], P.E.L. Clarke[46,37], M. Clemencic[37], H.V. Cliff[43], J. Closier[37], C. Coca[28],
V. Coco[23], J. Cogan[6], P. Collins[37], A. Comerma-Montells[35], F. Constantin[28], A. Contu[51],
A. Cook[42], M. Coombes[42], G. Corti[37], G.A. Cowan[38], R. Currie[46], C. D'Ambrosio[37],
P. David[8], P.N.Y. David[23], I. De Bonis[4], S. De Capua[21,k], M. De Cian[39], F. De Lorenzi[12],
J.M. De Miranda[1], L. De Paula[2], P. De Simone[18], D. Decamp[4], M. Deckenhoff[9],
H. Degaudenzi[38,37], L. Del Buono[8], C. Deplano[15], D. Derkach[14,37], O. Deschamps[5],
F. Dettori[24], J. Dickens[43], H. Dijkstra[37], P. Diniz Batista[1], F. Domingo Bonal[35,n],
S. Donleavy[48], F. Dordei[11], A. Dosil Suárez[36], D. Dossett[44], A. Dovbnya[40],
F. Dupertuis[38], R. Dzhelyadin[34], A. Dziurda[25], S. Easo[45], U. Egede[49], V. Egorychev[30],
S. Eidelman[33], D. van Eijk[23], F. Eisele[11], S. Eisenhardt[46], R. Ekelhof[9], L. Eklund[47],
Ch. Elsasser[39], D. Elsby[55], D. Esperante Pereira[36], L. Estève[43], A. Falabella[16,14,e],
E. Fanchini[20,j], C. Färber[11], G. Fardell[46], C. Farinelli[23], S. Farry[12], V. Fave[38],
V. Fernandez Albor[36], M. Ferro-Luzzi[37], S. Filippov[32], C. Fitzpatrick[46], M. Fontana[10],
F. Fontanelli[19,i], R. Forty[37], M. Frank[37], C. Frei[37], M. Frosini[17,f,37], S. Furcas[20],
A. Gallas Torreira[36], D. Galli[14,c], M. Gandelman[2], P. Gandini[51], Y. Gao[3], J-C. Garnier[37],
J. Garofoli[52], J. Garra Tico[43], L. Garrido[35], D. Gascon[35], C. Gaspar[37], N. Gauvin[38],
M. Gersabeck[37], T. Gershon[44,37], Ph. Ghez[4], V. Gibson[43], V.V. Gligorov[37], C. Göbel[54],
D. Golubkov[30], A. Golutvin[49,30,37], A. Gomes[2], H. Gordon[51], M. Grabalosa Gándara[35],
R. Graciani Diaz[35], L.A. Granado Cardoso[37], E. Graugés[35], G. Graziani[17], A. Grecu[28],
E. Greening[51], S. Gregson[43], B. Gui[52], E. Gushchin[32], Yu. Guz[34], T. Gys[37], G. Haefeli[38],
C. Haen[37], S.C. Haines[43], T. Hampson[42], S. Hansmann-Menzemer[11], R. Harji[49],
N. Harnew[51], J. Harrison[50], P.F. Harrison[44], T. Hartmann[56], J. He[7], V. Heijne[23],
K. Hennessy[48], P. Henrard[5], J.A. Hernando Morata[36], E. van Herwijnen[37], E. Hicks[48],

K. Holubyev[11], P. Hopchev[4], W. Hulsbergen[23], P. Hunt[51], T. Huse[48], R.S. Huston[12],
D. Hutchcroft[48], D. Hynds[47], V. Iakovenko[41], P. Ilten[12], J. Imong[42], R. Jacobsson[37],
A. Jaeger[11], M. Jahjah Hussein[5], E. Jans[23], F. Jansen[23], P. Jaton[38], B. Jean-Marie[7],
F. Jing[3], M. John[51], D. Johnson[51], C.R. Jones[43], B. Jost[37], M. Kaballo[9], S. Kandybei[40],
M. Karacson[37], T.M. Karbach[9], J. Keaveney[12], I.R. Kenyon[55], U. Kerzel[37], T. Ketel[24],
A. Keune[38], B. Khanji[6], Y.M. Kim[46], M. Knecht[38], P. Koppenburg[23], A. Kozlinskiy[23],
L. Kravchuk[32], K. Kreplin[11], M. Kreps[44], G. Krocker[11], P. Krokovny[11], F. Kruse[9],
K. Kruzelecki[37], M. Kucharczyk[20,25,37,j], T. Kvaratskheliya[30,37], V.N. La Thi[38],
D. Lacarrere[37], G. Lafferty[50], A. Lai[15], D. Lambert[46], R.W. Lambert[24], E. Lanciotti[37],
G. Lanfranchi[18], C. Langenbruch[11], T. Latham[44], C. Lazzeroni[55], R. Le Gac[6],
J. van Leerdam[23], J.-P. Lees[4], R. Lefèvre[5], A. Leflat[31,37], J. Lefrançois[7], O. Leroy[6],
T. Lesiak[25], L. Li[3], L. Li Gioi[5], M. Lieng[9], M. Liles[48], R. Lindner[37], C. Linn[11], B. Liu[3],
G. Liu[37], J. von Loeben[20], J.H. Lopes[2], E. Lopez Asamar[35], N. Lopez-March[38],
H. Lu[38,3], J. Luisier[38], A. Mac Raighne[47], F. Machefert[7], I.V. Machikhiliyan[4,30],
F. Maciuc[10], O. Maev[29,37], J. Magnin[1], S. Malde[51], R.M.D. Mamunur[37], G. Manca[15,d],
G. Mancinelli[6], N. Mangiafave[43], U. Marconi[14], R. Märki[38], J. Marks[11], G. Martellotti[22],
A. Martens[8], L. Martin[51], A. Martín Sánchez[7], D. Martinez Santos[37], A. Massafferri[1],
Z. Mathe[12], C. Matteuzzi[20], M. Matveev[29], E. Maurice[6], B. Maynard[52],
A. Mazurov[16,32,37], G. McGregor[50], R. McNulty[12], M. Meissner[11], M. Merk[23], J. Merkel[9],
R. Messi[21,k], S. Miglioranzi[37], D.A. Milanes[13,37], M.-N. Minard[4], J. Molina Rodriguez[54],
S. Monteil[5], D. Moran[12], P. Morawski[25], R. Mountain[52], I. Mous[23], F. Muheim[46],
K. Müller[39], R. Muresan[28,38], B. Muryn[26], B. Muster[38], M. Musy[35], J. Mylroie-Smith[48],
P. Naik[42], T. Nakada[38], R. Nandakumar[45], I. Nasteva[1], M. Nedos[9], M. Needham[46],
N. Neufeld[37], C. Nguyen-Mau[38,o], M. Nicol[7], V. Niess[5], N. Nikitin[31], A. Nomerotski[51],
A. Novoselov[34], A. Oblakowska-Mucha[26], V. Obraztsov[34], S. Oggero[23], S. Ogilvy[47],
O. Okhrimenko[41], R. Oldeman[15,d], M. Orlandea[28], J.M. Otalora Goicochea[2], P. Owen[49],
K. Pal[52], J. Palacios[39], A. Palano[13,b], M. Palutan[18], J. Panman[37], A. Papanestis[45],
M. Pappagallo[47], C. Parkes[50,37], C.J. Parkinson[49], G. Passaleva[17], G.D. Patel[48],
M. Patel[49], S.K. Paterson[49], G.N. Patrick[45], C. Patrignani[19,i], C. Pavel-Nicorescu[28],
A. Pazos Alvarez[36], A. Pellegrino[23], G. Penso[22,l], M. Pepe Altarelli[37], S. Perazzini[14,c],
D.L. Perego[20,j], E. Perez Trigo[36], A. Pérez-Calero Yzquierdo[35], P. Perret[5],
M. Perrin-Terrin[6], G. Pessina[20], A. Petrella[16,37], A. Petrolini[19,i], A. Phan[52],
E. Picatoste Olloqui[35], B. Pie Valls[35], B. Pietrzyk[4], T. Pilař[44], D. Pinci[22], R. Plackett[47],
S. Playfer[46], M. Plo Casasus[36], G. Polok[25], A. Poluektov[44,33], E. Polycarpo[2], D. Popov[10],
B. Popovici[28], C. Potterat[35], A. Powell[51], J. Prisciandaro[38], V. Pugatch[41],
A. Puig Navarro[35], W. Qian[52], J.H. Rademacker[42], B. Rakotomiaramanana[38],
M.S. Rangel[2], I. Raniuk[40], G. Raven[24], S. Redford[51], M.M. Reid[44], A.C. dos Reis[1],
S. Ricciardi[45], K. Rinnert[48], D.A. Roa Romero[5], P. Robbe[7], E. Rodrigues[47,50],
F. Rodrigues[2], P. Rodriguez Perez[36], G.J. Rogers[43], S. Roiser[37], V. Romanovsky[34],
M. Rosello[35,n], J. Rouvinet[38], T. Ruf[37], H. Ruiz[35], G. Sabatino[21,k], J.J. Saborido Silva[36],
N. Sagidova[29], P. Sail[47], B. Saitta[15,d], C. Salzmann[39], M. Sannino[19,i], R. Santacesaria[22],
C. Santamarina Rios[36], R. Santinelli[37], E. Santovetti[21,k], M. Sapunov[6], A. Sarti[18,l],
C. Satriano[22,m], A. Satta[21], M. Savrie[16,e], D. Savrina[30], P. Schaack[49], M. Schiller[24],

S. Schleich[9], M. Schlupp[9], M. Schmelling[10], B. Schmidt[37], O. Schneider[38],
A. Schopper[37], M.-H. Schune[7], R. Schwemmer[37], B. Sciascia[18], A. Sciubba[18,l], M. Seco[36],
A. Semennikov[30], K. Senderowska[26], I. Sepp[49], N. Serra[39], J. Serrano[6], P. Seyfert[11],
M. Shapkin[34], I. Shapoval[40,37], P. Shatalov[30], Y. Shcheglov[29], T. Shears[48],
L. Shekhtman[33], O. Shevchenko[40], V. Shevchenko[30], A. Shires[49], R. Silva Coutinho[44],
T. Skwarnicki[52], A.C. Smith[37], N.A. Smith[48], E. Smith[51,45], K. Sobczak[5], F.J.P. Soler[47],
A. Solomin[42], F. Soomro[18], B. Souza De Paula[2], B. Spaan[9], A. Sparkes[46], P. Spradlin[47],
F. Stagni[37], S. Stahl[11], O. Steinkamp[39], S. Stoica[28], S. Stone[52,37], B. Storaci[23],
M. Straticiuc[28], U. Straumann[39], V.K. Subbiah[37], S. Swientek[9], M. Szczekowski[27],
P. Szczypka[38], T. Szumlak[26], S. T'Jampens[4], E. Teodorescu[28], F. Teubert[37],
C. Thomas[51], E. Thomas[37], J. van Tilburg[11], V. Tisserand[4], M. Tobin[39],
S. Topp-Joergensen[51], N. Torr[51], E. Tournefier[4,49], M.T. Tran[38], A. Tsaregorodtsev[6],
N. Tuning[23], M. Ubeda Garcia[37], A. Ukleja[27], P. Urquijo[52], U. Uwer[11], V. Vagnoni[14],
G. Valenti[14], R. Vazquez Gomez[35], P. Vazquez Regueiro[36], S. Vecchi[16], J.J. Velthuis[42],
M. Veltri[17,g], B. Viaud[7], I. Videau[7], X. Vilasis-Cardona[35,n], J. Visniakov[36],
A. Vollhardt[39], D. Volyanskyy[10], D. Voong[42], A. Vorobyev[29], H. Voss[10],
S. Wandernoth[11], J. Wang[52], D.R. Ward[43], N.K. Watson[55], A.D. Webber[50],
D. Websdale[49], M. Whitehead[44], D. Wiedner[11], L. Wiggers[23], G. Wilkinson[51],
M.P. Williams[44,45], M. Williams[49], F.F. Wilson[45], J. Wishahi[9], M. Witek[25],
W. Witzeling[37], S.A. Wotton[43], K. Wyllie[37], Y. Xie[46], F. Xing[51], Z. Xing[52], Z. Yang[3],
R. Young[46], O. Yushchenko[34], M. Zavertyaev[10,a], F. Zhang[3], L. Zhang[52], W.C. Zhang[12],
Y. Zhang[3], A. Zhelezov[11], L. Zhong[3], E. Zverev[31], A. Zvyagin[37].

[1]*Centro Brasileiro de Pesquisas Físicas (CBPF), Rio de Janeiro, Brazil*
[2]*Universidade Federal do Rio de Janeiro (UFRJ), Rio de Janeiro, Brazil*
[3]*Center for High Energy Physics, Tsinghua University, Beijing, China*
[4]*LAPP, Université de Savoie, CNRS/IN2P3, Annecy-Le-Vieux, France*
[5]*Clermont Université, Université Blaise Pascal, CNRS/IN2P3, LPC, Clermont-Ferrand, France*
[6]*CPPM, Aix-Marseille Université, CNRS/IN2P3, Marseille, France*
[7]*LAL, Université Paris-Sud, CNRS/IN2P3, Orsay, France*
[8]*LPNHE, Université Pierre et Marie Curie, Université Paris Diderot, CNRS/IN2P3, Paris, France*
[9]*Fakultät Physik, Technische Universität Dortmund, Dortmund, Germany*
[10]*Max-Planck-Institut für Kernphysik (MPIK), Heidelberg, Germany*
[11]*Physikalisches Institut, Ruprecht-Karls-Universität Heidelberg, Heidelberg, Germany*
[12]*School of Physics, University College Dublin, Dublin, Ireland*
[13]*Sezione INFN di Bari, Bari, Italy*
[14]*Sezione INFN di Bologna, Bologna, Italy*
[15]*Sezione INFN di Cagliari, Cagliari, Italy*
[16]*Sezione INFN di Ferrara, Ferrara, Italy*
[17]*Sezione INFN di Firenze, Firenze, Italy*
[18]*Laboratori Nazionali dell'INFN di Frascati, Frascati, Italy*
[19]*Sezione INFN di Genova, Genova, Italy*
[20]*Sezione INFN di Milano Bicocca, Milano, Italy*
[21]*Sezione INFN di Roma Tor Vergata, Roma, Italy*
[22]*Sezione INFN di Roma La Sapienza, Roma, Italy*
[23]*Nikhef National Institute for Subatomic Physics, Amsterdam, The Netherlands*
[24]*Nikhef National Institute for Subatomic Physics and Vrije Universiteit, Amsterdam, The Netherlands*
[25]*Henryk Niewodniczanski Institute of Nuclear Physics Polish Academy of Sciences, Kraców, Poland*

[26] AGH University of Science and Technology, Kraców, Poland

[27] Soltan Institute for Nuclear Studies, Warsaw, Poland

[28] Horia Hulubei National Institute of Physics and Nuclear Engineering, Bucharest-Magurele, Romania

[29] Petersburg Nuclear Physics Institute (PNPI), Gatchina, Russia

[30] Institute of Theoretical and Experimental Physics (ITEP), Moscow, Russia

[31] Institute of Nuclear Physics, Moscow State University (SINP MSU), Moscow, Russia

[32] Institute for Nuclear Research of the Russian Academy of Sciences (INR RAN), Moscow, Russia

[33] Budker Institute of Nuclear Physics (SB RAS) and Novosibirsk State University, Novosibirsk, Russia

[34] Institute for High Energy Physics (IHEP), Protvino, Russia

[35] Universitat de Barcelona, Barcelona, Spain

[36] Universidad de Santiago de Compostela, Santiago de Compostela, Spain

[37] European Organization for Nuclear Research (CERN), Geneva, Switzerland

[38] Ecole Polytechnique Fédérale de Lausanne (EPFL), Lausanne, Switzerland

[39] Physik-Institut, Universität Zürich, Zürich, Switzerland

[40] NSC Kharkiv Institute of Physics and Technology (NSC KIPT), Kharkiv, Ukraine

[41] Institute for Nuclear Research of the National Academy of Sciences (KINR), Kyiv, Ukraine

[42] H.H. Wills Physics Laboratory, University of Bristol, Bristol, United Kingdom

[43] Cavendish Laboratory, University of Cambridge, Cambridge, United Kingdom

[44] Department of Physics, University of Warwick, Coventry, United Kingdom

[45] STFC Rutherford Appleton Laboratory, Didcot, United Kingdom

[46] School of Physics and Astronomy, University of Edinburgh, Edinburgh, United Kingdom

[47] School of Physics and Astronomy, University of Glasgow, Glasgow, United Kingdom

[48] Oliver Lodge Laboratory, University of Liverpool, Liverpool, United Kingdom

[49] Imperial College London, London, United Kingdom

[50] School of Physics and Astronomy, University of Manchester, Manchester, United Kingdom

[51] Department of Physics, University of Oxford, Oxford, United Kingdom

[52] Syracuse University, Syracuse, NY, United States

[53] CC-IN2P3, CNRS/IN2P3, Lyon-Villeurbanne, France, associated member

[54] Pontifícia Universidade Católica do Rio de Janeiro (PUC-Rio), Rio de Janeiro, Brazil, associated to [2]

[55] University of Birmingham, Birmingham, United Kingdom

[56] Physikalisches Institut, Universität Rostock, Rostock, Germany, associated to [11]

[a] P.N. Lebedev Physical Institute, Russian Academy of Science (LPI RAS), Moscow, Russia

[b] Università di Bari, Bari, Italy

[c] Università di Bologna, Bologna, Italy

[d] Università di Cagliari, Cagliari, Italy

[e] Università di Ferrara, Ferrara, Italy

[f] Università di Firenze, Firenze, Italy

[g] Università di Urbino, Urbino, Italy

[h] Università di Modena e Reggio Emilia, Modena, Italy

[i] Università di Genova, Genova, Italy

[j] Università di Milano Bicocca, Milano, Italy

[k] Università di Roma Tor Vergata, Roma, Italy

[l] Università di Roma La Sapienza, Roma, Italy

[m] Università della Basilicata, Potenza, Italy

[n] LIFAELS, La Salle, Universitat Ramon Llull, Barcelona, Spain

[o] Hanoi University of Science, Hanoi, Viet Nam

1   Introduction

An important goal of heavy flavour experiments is to measure the mixing-induced CP violation phase in $\overline{B}{}^0_s$ decays, ϕ_s. As this phase is predicted to be small in the Standard Model (SM) [1], new physics can induce large changes [2]. Here we use the decay mode $\overline{B}{}^0_s \to J/\psi f_0(980)$. If only the dominant decay diagrams shown in Fig. 1 contribute, then the value of ϕ_s using $\overline{B}{}^0_s \to J/\psi f_0(980)$ is the same as that measured using $\overline{B}{}^0_s \to J/\psi \phi$ decay.
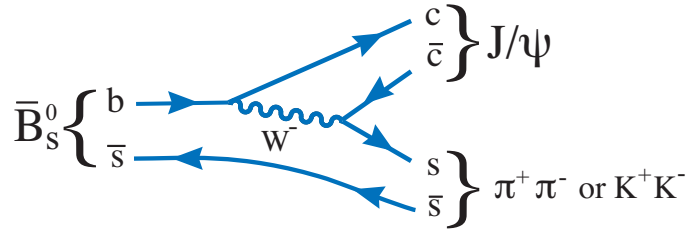
Figure 1: Dominant decay diagrams for $\overline{B}{}^0_s \to J/\psi f_0(980)$ or $J/\psi \phi$ decays.

Motivated by a prediction in Ref. [3], LHCb searched for and made the first observation of $\overline{B}{}^0_s \to J/\psi f_0(980)$ decays [4] that was subsequently confirmed by other experiments [5, 6]. Time dependent CP violation can be measured without an angular analysis, as the final state is a CP eigenstate. From now on f_0 will stand only for $f_0(980)$.

In the Standard Model, in terms of CKM matrix elements, $\phi_s = -2 \arg\left[\frac{V_{ts} V_{tb}^*}{V_{cs} V_{cb}^*}\right]$. The equations below are written assuming that there is only one decay amplitude, ignoring possible small contributions from other diagrams [7]. The decay time evolutions for initial B^0_s and $\overline{B}{}^0_s$ are [8]

$$\Gamma\left(\overset{(-)}{B^0_s} \to J/\psi f_0\right) = \mathcal{N} e^{-\Gamma_s t}\left\{e^{\Delta\Gamma_s t/2}(1 + \cos\phi_s) + e^{-\Delta\Gamma_s t/2}(1 - \cos\phi_s)\right.$$
$$\left. \pm \sin\phi_s \sin(\Delta m_s\, t)\right\}, \tag{1}$$

where $\Delta\Gamma_s$ is the decay width difference between light and heavy mass eigenstates, $\Delta\Gamma_s = \Gamma_{\mathrm{L}} - \Gamma_{\mathrm{H}}$. The decay width Γ_s is the average of the widths Γ_{L} and Γ_{H}, and $\mathcal{N}$ is a time-independent normalization factor. The plus sign in front of the $\sin\phi_s$ term applies to an initial $\overline{B}{}^0_s$ and the minus sign for an initial B^0_s meson. The time evolution of the untagged rate is then

$$\Gamma\left(B^0_s \to J/\psi f_0\right) + \Gamma\left(\overline{B}{}^0_s \to J/\psi f_0\right) = \mathcal{N} e^{-\Gamma_s t}\left\{e^{\Delta\Gamma_s t/2}(1 + \cos\phi_s) + e^{-\Delta\Gamma_s t/2}(1 - \cos\phi_s)\right\}. \tag{2}$$

Note that there is information in the shape of the lifetime distribution that correlates $\Delta\Gamma_s$ and ϕ_s. In this analysis we will use both samples of flavour tagged and untagged decays. Both Eqs. 1 and 2 are insensitive to the change $\phi_s \to \pi - \phi_s$ when $\Delta\Gamma_s \to -\Delta\Gamma_s$.

2 Selection requirements

We use a data sample of $0.41\,\mathrm{fb}^{-1}$ collected in 2010 and the first half of 2011 at a centre-of-mass energy of 7 TeV. This analysis is restricted to events accepted by a $J/\psi \to \mu^+\mu^-$ trigger. The LHCb detector and the track reconstruction are described in Ref. [9]. The detector elements most important for this analysis are the VELO, a silicon strip device that surrounds the pp interaction region, and other tracking devices. Two Ring Imaging Cherenkov (RICH) detectors are used to identify charged hadrons, while muons are identified using their penetration through iron.

To be considered a $J/\psi \to \mu^+\mu^-$ candidate particles of opposite charge are required to have transverse momentum, p_{T}, greater than 500 MeV, be identified as muons, and form a vertex with fit χ^2 per number of degrees of freedom (ndof) less than 11. We work in units where $c = \hbar = 1$. Only candidates with dimuon invariant mass between -48 MeV to $+43$ MeV of the J/ψ mass peak are selected. Pion candidates are selected if they are inconsistent with having been produced at the primary vertex. The impact parameter (IP) is the minimum distance of approach of the track with respect to the primary vertex. We require that the χ^2 formed by using the hypothesis that the IP is zero be > 9 for each track. For further consideration particles forming di-pion candidates must be positively identified in the RICH system, and must have their scalar sum $p_{\mathrm{T}} > 900\,\mathrm{MeV}$.

To select $\overline{B}_s^0$ candidates we further require that the two pions form a vertex with a $\chi^2 < 10$, that they form a candidate $\overline{B}_s^0$ vertex with the J/ψ where the vertex fit $\chi^2/\mathrm{ndof} < 5$, that this vertex is $> 1.5\,\mathrm{mm}$ from the primary, and points to the primary vertex at an angle not different from its momentum direction by more than 11.8 mrad.

The invariant mass of selected $\mu^+\mu^-\pi\pi$ combinations, where the di-muon pair is constrained to have the J/ψ mass, is shown in Fig. 2 for both opposite-sign and like-sign di-pion combinations, requiring di-pion invariant masses within 90 MeV of 980 MeV. Here like-sign combinations are defined as the sum of $\pi^+\pi^+$ and $\pi^-\pi^-$ candidates. The signal shape, the same for both $\overline{B}_s^0$ and $\overline{B}^0$, is a double-Gaussian, where the core Gaussian's mean and width are allowed to vary, and the fraction and width ratio for the second Gaussian are fixed to the values obtained in a separate fit to $\overline{B}_s^0 \to J/\psi\phi$. The mean values of both Gaussians are required to be the same. The combinatoric background is described by an exponential function. Other background components are $B^- \to J/\psi h^-$, where h^- can be either a K^- or a π^- and an additional π^+ is found, $\overline{B}_s^0 \to J/\psi\eta'$, $\eta' \to \rho\gamma$, $\overline{B}_s^0 \to J/\psi\phi$, $\phi \to \pi^+\pi^-\pi^0$, and $\overline{B}^0 \to J/\psi\overline{K}^{*0}$. The shapes for these background sources are taken from Monte Carlo simulation based on PYTHIA [10] and GEANT-4 [11] with their normalizations allowed to vary. We performed a simultaneous fit to the opposite-sign and like-sign di-pion event distributions. There are 1428 ± 47 signal events within $\pm20\,\mathrm{MeV}$ of the $\overline{B}_s^0$ mass peak. The background under the peak in this interval is 467 ± 11 events, giv-

ing a signal purity of 75%. Importantly, the like-sign di-pion yield at masses higher than the $\overline{B}_s^0$ gives an excellent description of the shape and level of the background. Simulation studies have demonstrated that it also describes the background under the peak.
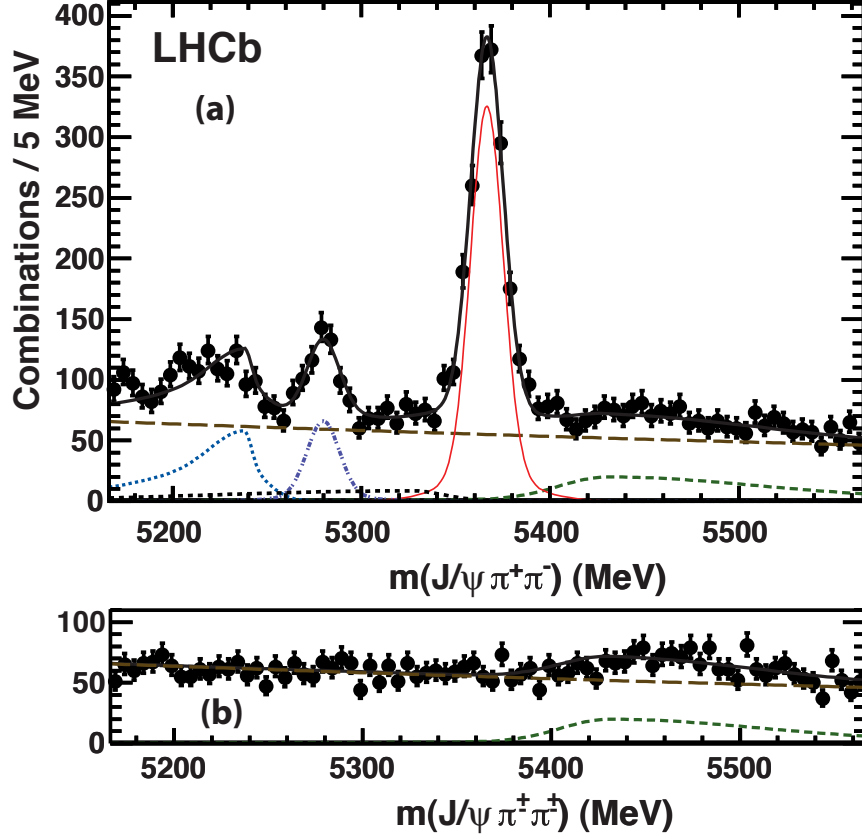

Figure 2: (a) Invariant mass of $J/\psi\pi^+\pi^-$ combinations when the $\pi^+\pi^-$ pair is required to be within ± 90 MeV of the nominal $f_0(980)$ mass. The data have been fitted with a double-Gaussian signal and several background functions. The thin (red) solid line shows the signal, the long-dashed (brown) line the combinatoric background, the dashed (green) line the B^- background (mostly at masses above the signal peak), the dotted (blue) line the $\overline{B}^0 \to J/\psi\overline{K}^{*0}$ background, the dash-dot line (purple) the $\overline{B}^0 \to J/\psi\pi^+\pi^-$ background, the dotted line (black) the sum of $\overline{B}_s^0 \to J/\psi\eta'$ and $J/\psi\phi$ backgrounds (barely visible), and the thick-solid (black) line the total. (b) The mass distribution for like-sign candidates.

The invariant mass of di-pion combinations is shown in Fig. 3 for both opposite-sign and like-sign di-pion combinations within ± 20 MeV of the $\overline{B}_s^0$ candidate mass peak. A large signal is present near the nominal $f_0(980)$ mass. Other $\overline{B}_s^0 \to J/\psi\pi^+\pi^-$ signal events are present at higher masses. In what follows we only use events in the f_0 signal region from 890 to 1070 MeV.
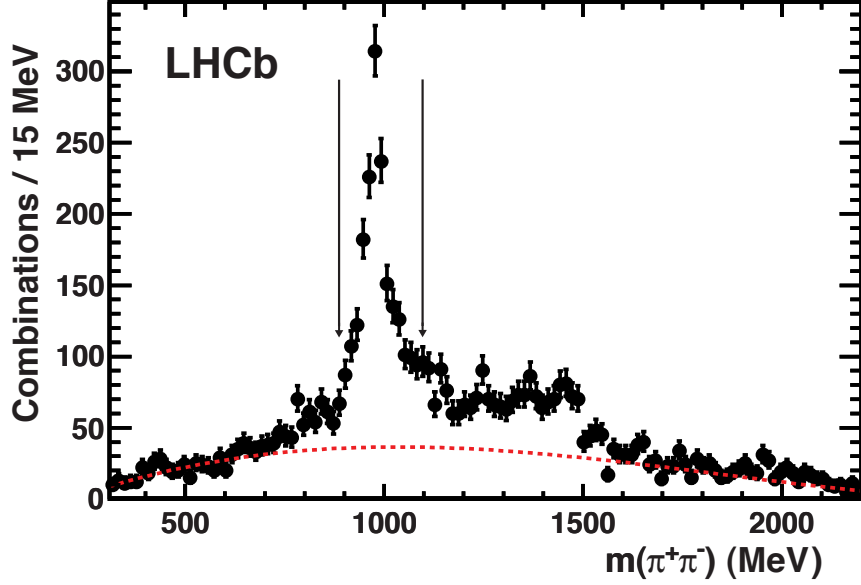
3

Figure 3: Invariant mass of $\pi^+\pi^-$ combinations (points) and a fit to the $\pi^\pm\pi^\pm$ data (dashed line) for events in the $\bar{B}_s^0$ signal region. The region between the vertical arrows contains the events selected for further analysis.

3 S-wave content

Since the initial isospin of the $s\bar{s}$ system that produces the two pions is zero, and since the G-parity of the two pions is even, only even spin is allowed for the $\pi^+\pi^-$ pair. Since no spin-4 resonances have been observed below 2 GeV, the angular distributions are described by the coherent combination of spin-0 and spin-2 resonant decays. We use the helicity basis and define the decay angles as $\theta_{J/\psi}$, the angle of the μ^+ in the J/ψ rest frame with respect to the $\bar{B}_s^0$ direction, and θ_{f_0}, the angle of the π^+ in the $\pi^+\pi^-$ rest frame with respect to the $\bar{B}_s^0$ direction. The spin-0 amplitude is labeled as A_{00}, the three spin-2 amplitudes as A_{2i}, $i = -1, 0, 1$, and δ is the strong phase between the A_{20} and A_{00} amplitudes.

After integrating over the angle between the two decay planes the joint angular distribution is given by [12]

$$\frac{d\Gamma}{d\cos\theta_{f_0}d\cos\theta_{J/\psi}} = \left| A_{00} + \frac{1}{2}A_{20}e^{i\delta}\sqrt{5}\left(3\cos^2\theta_{f_0} - 1\right)\right|^2 \sin^2\theta_{J/\psi}$$
$$+ \frac{1}{4}\left(|A_{21}|^2 + |A_{2-1}|^2\right)\left(15\sin^2\theta_{f_0}\cos^2\theta_{f_0}\right)\left(1 + \cos^2\theta_{J/\psi}\right). \quad (3)$$

Since the $\bar{B}_s^0$ is spinless, when it decays into a spin-1 J/ψ and a spin-0 f_0, $\theta_{J/\psi}$ should be distributed as $\sin^2\theta_{J/\psi}$ and $\cos\theta_{f_0}$ should be uniformly distributed.

The helicity distributions of the opposite-sign data selected with reconstructed $J/\psi\pi^+\pi^-$ mass within $\pm 20\,\text{MeV}$ of the known $\bar{B}_s^0$ mass and within $\pm 90\,\text{MeV}$ of the nominal $f_0(980)$ mass, are shown in Fig. 4; the data have been background subtracted, using

4

the like-sign data, and acceptance corrected using Monte Carlo simulation. We perform a two-dimensional unbinned angular fit. The ratio of rates is found to be

$$\frac{|A_{20}|^2}{|A_{00}|^2} = (0.1^{+2.6}_{-0.1})\%,$$

$$\frac{|A_{21}|^2 + |A_{2-1}|^2}{|A_{00}|^2} = (0.0^{+1.7}_{-0.0})\%, \tag{4}$$

where the uncertainties are statistical only. The spin-2 amplitudes are consistent with zero. Note that the A_{20} amplitude corresponds to CP odd final states, and thus would exhibit the same CP violating phase as the $J/\psi f_0$ final state, while the $A_{2\pm1}$ amplitude can be either CP odd or even. Thus this sample is taken as pure CP odd.
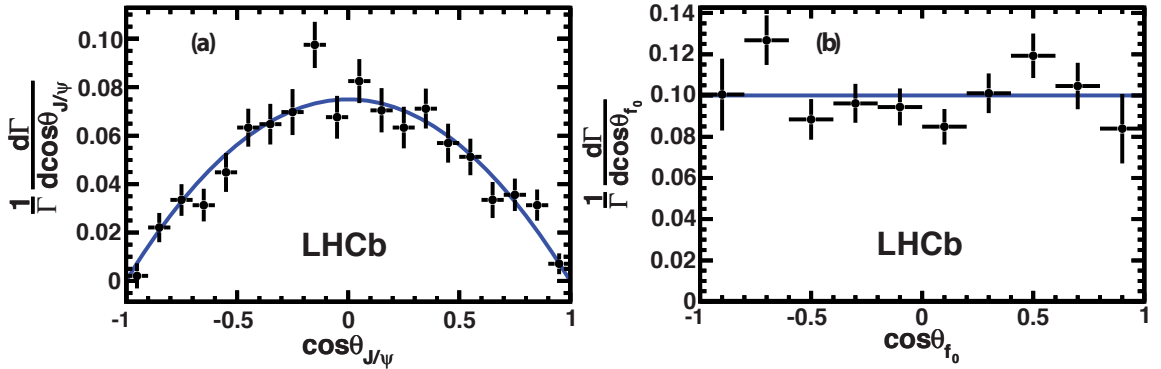

Figure 4: Efficiency corrected, background subtracted angular distributions in the $\pi^+\pi^-$ mass region within $\pm90\,\mathrm{MeV}$ of $980\,\mathrm{MeV}$ and within ±20 MeV of the $\overline{B}^0_s$ mass for (a) $\cos^2\theta_{J/\psi}$, and (b) $\cos\theta_{f_0}$. The solid lines show the expectations for a spin-0 object.

4   Time resolution and acceptance

The $\overline{B}^0_s$ decay time is defined here as $t = m\,\vec{d}\cdot\vec{p}/|\vec{p}|^2$, where m is the reconstructed invariant mass, $\vec{p}$ the momentum and $\vec{d}$ the flight vector of the candidate $\overline{B}^0_s$ from the primary to the secondary vertices. If more than one primary vertex is found, the one that corresponds to the smallest IP χ^2 of the $\overline{B}^0_s$ candidate is chosen.

The decay time resolution probability distribution function (PDF) is determined from data using J/ψ detected without any requirement on detachment from the primary vertex (prompt) plus two oppositely charged particles from the primary vertex with the same selection criteria as for $J/\psi f_0$ events, except for the IP χ^2 requirement. Monte Carlo simulation shows that the time resolution PDF is well modelled by these events. Fig. 5 shows the t distribution for our $J/\psi\pi^+\pi^-$ prompt 2011 data sample. To describe the background time distribution three components are needed, (i) prompt, (ii) a small long lived background ($f_{\mathrm{LL1}} = 2.64 \pm 0.10$)% modeled by an exponential decay function, and

(iii) an even smaller component ($f_{\mathrm{LL2}} = 0.46 \pm 0.02$)% from b-hadron decay described by an additional exponential. Each of these are convolved individually with a triple-Gaussian resolution function with common means, whose components are listed in Table 1. The overall equivalent time resolution is $\sigma_t = 38.4$ fs.

The functional form for the time dependence is given by

$$
\begin{aligned}
N(t) \;=\; & (1 - f_{\mathrm{LL1}} - f_{\mathrm{LL2}}) \cdot 3G + f_{\mathrm{LL1}} \left[\frac{1}{\tau_1} \exp(-t/\tau_1) \otimes 3G \right] \\
& + f_{\mathrm{LL2}} \cdot [1/\tau_2 \cdot \exp(-t/\tau_2) \otimes 3G].
\end{aligned}
\tag{5}
$$

The fractions f_{LL1} and f_{LL2} , and their respective lifetimes τ_1 and τ_2, are varied in the fit. The parameters of the triple-Gaussian time resolution, $3G$, are listed in Table 1. The symbol $\otimes$ indicates a convolution.
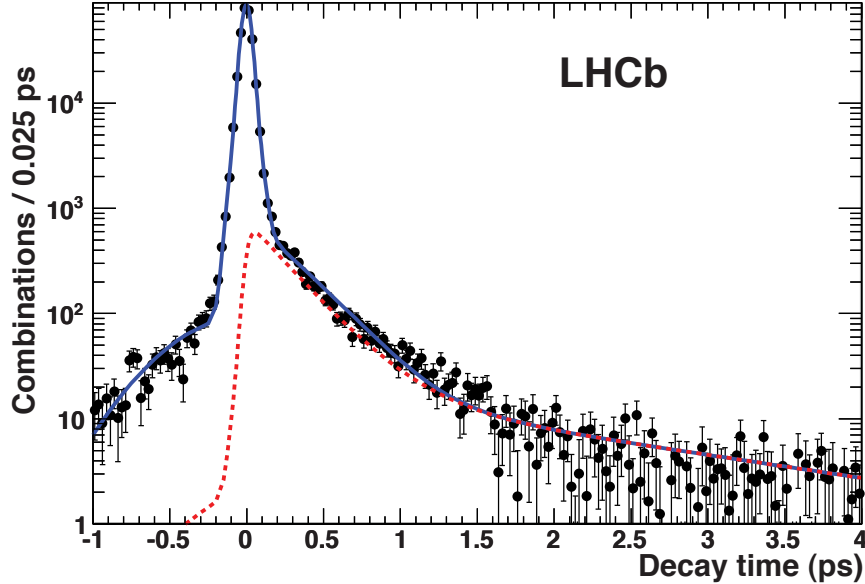

Figure 5: Decay time distribution for prompt $J/\psi\pi^+\pi^-$ events. The dashed line (red) shows the long lived components, while the solid line (blue) shows the total.

A decay time acceptance is introduced by the triggering and event selection requirements. Monte Carlo simulations show that the shape of the decay time acceptance function is well modelled by

$$
A(t) = C \frac{[a\,(t - t_0)]^n}{1 + [a\,(t - t_0)]^n} \quad ,
\tag{6}
$$

where C is a normalization constant. Furthermore, the parameter values are found to be the same for simulated $\overline{B}^0 \to J/\psi\overline{K}^{*0}$ events with $\overline{K}^{*0} \to K^-\pi^+$, as for $\overline{B}^0_s \to J/\psi f_0$.

Fig. 6(a) shows the $J/\psi\overline{K}^{*0}$ mass distribution in data with an additional requirement that the kaon candidate be positively identified in the RICH system, and that the $K^-\pi^+$ invariant mass be within $\pm100\,\mathrm{MeV}$ of 892 MeV. There are 36881 ± 208 signal events.

The sideband subtracted decay time distribution is shown in Fig. 6(b) and fit using the above defined acceptance function gives values of $a = (1.89 \pm 0.07)\,\mathrm{ps}^{-1}$, $n = 1.84 \pm 0.12$, $t_0 = (0.127 \pm 0.015)\,\mathrm{ps}$, and also a value of the $\overline{B}^0$ lifetime of $1.510 \pm 0.016\,\mathrm{ps}$, where the error is statistical only. This is in good agreement with the PDG average of $1.519 \pm 0.007\,\mathrm{ps}$ [13].
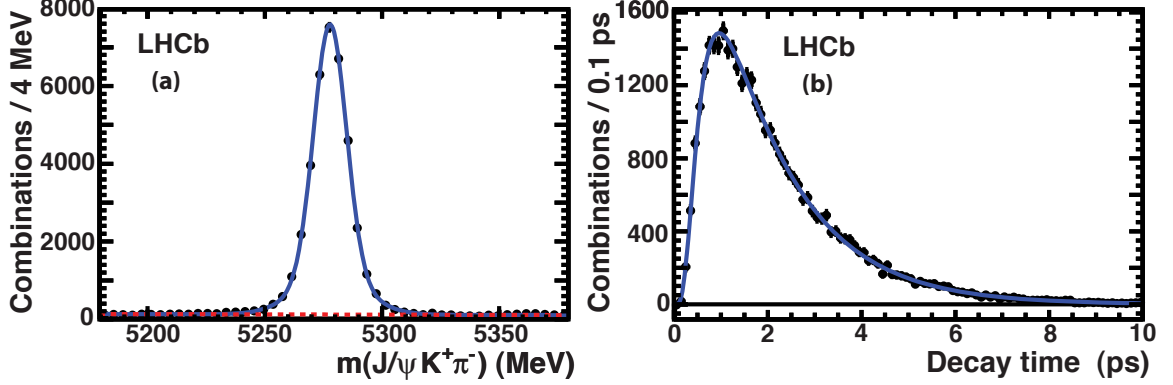

Figure 6: Distributions for $\overline{B}^0 \to J/\psi \overline{K}^{*0}$ events (a) $\overline{B}^0$ candidate mass distribution and (b) decay time distribution, where the small background has been subtracted using the $\overline{B}^0$ candidate mass sidebands.

Another check is provided by a recent CDF lifetime measurement of $\overline{B}^0_s \to J/\psi f_0$ of $1.70^{+0.12}_{-0.11} \pm 0.03\,\mathrm{ps}$ obtained by fitting the data to a single exponential [6]. Such a fit to our data yields $1.68 \pm 0.05\,\mathrm{ps}$, where the uncertainty is only statistical.

5 Fit strategy

5.1 Likelihood function characterization

The selected events are used to maximize a likelihood function

$$\mathcal{L} = \prod_i^N P(m_i, t_i, q_i),\tag{7}$$

where m_i is the reconstructed candidate $\overline{B}^0_s$ mass, t_i the decay time, and N the total number of events. The flavour tag, q_i, takes values of $+1$, -1 and 0, respectively, if the signal meson is tagged as B^0_s, $\overline{B}^0_s$, or untagged. The likelihood contains three components: signal, long-lived (LL) background and short-lived (SL) background.

For tagged events we have

$$
\begin{aligned}
P(m_i, t_i, q_i) =\ & N_{\mathrm{sig}} \epsilon_{\mathrm{sig}}^{\mathrm{tag}} P_m^{\mathrm{sig}}(m_i) P_t^{\mathrm{sig}}(t_i, q_i) \\
& + N_{\mathrm{LL}} \epsilon_{\mathrm{LL}}^{\mathrm{tag}} P_m^{\mathrm{bkg}}(m_i) P_t^{\mathrm{LL}}(t_i) + N_{\mathrm{SL}} \epsilon_{\mathrm{SL}}^{\mathrm{tag}} P_m^{\mathrm{bkg}}(m_i) P_t^{\mathrm{SL}}(t_i),
\end{aligned}
\tag{8}
$$

where: (i) $P_m^{\mathrm{sig}}(m_i)$ and $P_m^{\mathrm{bkg}}(m_i)$ are the PDFs describing the dependence on reconstructed mass m_i for signal and background events; (ii) $P_t^{\mathrm{sig}}(t_i, q_i)$ is the PDF used to describe the signal decay rates for the decay time t_i; (iii) $P_t^{\mathrm{LL}}(t_i)$ is the PDF describing the long-lived background decay rates, and $P_t^{\mathrm{SL}}(t_i)$ describes the short-lived background, both of which do not depend on the tagging; (iv) ϵ^{tag} refers to the respective tagging efficiencies for signal, long-lived and short-lived backgrounds.

For untagged events we have

$$
\begin{aligned}
P(m_i, t_i, 0) \quad &= N_{\mathrm{sig}}(1 - \epsilon_{\mathrm{sig}}^{\mathrm{tag}}) P_m^{\mathrm{sig}}(m_i) P_t^{\mathrm{sig}}(t_i, 0) \\
&+ N_{\mathrm{LL}}(1 - \epsilon_{\mathrm{LL}}^{\mathrm{tag}}) P_m^{\mathrm{bkg}}(m_i) P_t^{\mathrm{LL}}(t_i) + N_{\mathrm{SL}}(1 - \epsilon_{\mathrm{SL}}^{\mathrm{tag}}) P_m^{\mathrm{bkg}}(m_i) P_t^{\mathrm{SL}}(t_i). \quad (9)
\end{aligned}
$$

The total yields of the signal and background components are fixed to the number of events determined from the fit to the mass distributions (see Sec. 2). For both, the PDF is a product which models the invariant mass distribution and the time-dependent decay rates. The $\overline{B}_s^0$ mass spectrum is described by a double-Gaussian for the signal and an exponential function for the background (see Fig. 2). From Eqs. 1 and 2, the decay time function for the signal is

$$
R(t, q_i) \propto e^{-\Gamma_s t} \left\{ \cosh \frac{\Delta\Gamma_s t}{2} + \cos\phi_s \sinh \frac{\Delta\Gamma_s t}{2} - q_i D \sin\phi_s \sin(\Delta m_s t) \right\}. \quad (10)
$$

The probability of a wrong tag, ω, is included in the dilution factor $D \equiv (1 - 2\omega)$ (see Section 5.2).

The signal PDF is taken as a product of the decay time function, $R(t, q_i)$, convolved with the triple Gaussian time resolution function multiplied with the time acceptance function found from $J/\psi K^{*0}$ discussed in Section 4. The background decay time PDFs are determined using the like-sign $\pi^{\pm}\pi^{\pm}$ combinations. The time distribution of the like-sign background agrees in both yield and shape with the opposite-sign events in the upper $\overline{B}_s^0$ mass candidate sideband $50-200\,\mathrm{MeV}$ above the mass peak.

The background functions and parameters are listed in Table 1. The short-lived background component results from combining prompt J/ψ events with a opposite-sign pion pair that is not rejected by our selection requirements. The long-lived part constitutes $\approx 85\%$ of the background.

Table 1: The PDFs for the invariant mass and proper time describing the signal and background. P_t^{sig} refers to the decay time distribution in Eq. 9 and A is given in Eq. 6. Where two numbers are listed, the first refers to the 2011 data and the second to the 2010 data. If only one number is listed they are the same for both years. The symbol $\hat{t}$ refers to the true time.

P_m	P_t
Signal	
Double-Gaussian ($2G$)	$P_t^{\text{sig}}(t,q) = R(\hat{t},q) \otimes 3G(t-\hat{t}; \mu, \sigma_1^t, \sigma_2^t, \sigma_3^t, f_2^t, f_3^t)$
$2G(m; m_0, \sigma_1, \sigma_2, f_2)$	$\cdot A(t; a, n, t_0)$
$m_0 = 5366.5(3)$ MeV	$\mu = -0.0021(1)$ ps, $-0.0011(1)$ ps
$\sigma_1 = 8.6(3)$ MeV	$\sigma_1^t = 0.0300(4)$ ps, $0.0295(5)$ ps
$\sigma_2 = 26.8(9)$ MeV	$\sigma_2^t/\sigma_1^t = 1.92(4)$, $1.88(3)$
$f_2 = 0.14(2)$	$\sigma_3^t/\sigma_1^t = 14.6(10)$, $14.0(9)$
	$f_2^t = 0.23(2)$, $0.27(3)$
	$f_3^t = 0.0136(6)$, $0.0121(7)$
	$a = 1.89(7)$ ps^{-1}, $n = 1.84(12)$, $t_0 = 0.127(15)$ ps
Long-lived background	
Exponential	$[e^{-\hat{t}/\tau^{\text{bkg}}} \otimes 2G(t-\hat{t}; \mu, \sigma_1^t, \sigma_2^t, f_2^t)] \cdot A(t; a, n, t_0)$
	$\mu = 0$
	$\sigma_1^t = 0.088$ ps
	$\sigma_2^t = 5.94$ ps
	$f_2^t = 0.0137$
	$\tau^{\text{bkg}} = 0.96$ ps
	$a = 4.44$ ps^{-1}, $n = 4.56$, $t_0 = 0$ ps
Short-lived background	
Exponential	$2G(t; \mu, \sigma_1^t, \sigma_2^t, f_2^t) \cdot A(t; a, n, t_0)$
	All parameters are the same as for LL background

5.2 Flavour tagging

Flavour tagging uses decays of the other b hadron in the event, exploiting information from several sources including high transverse momentum muons, electrons and kaons, and the charge of inclusively reconstructed secondary vertices. The decisions of the four tagging algorithms are individually calibrated using $B^- \rightarrow J/\psi K^-$ decays and combined [14]. The effective tagging performance is characterized by $\epsilon_{\mathrm{sig}}^{\mathrm{tag}} D^2$, where $\epsilon_{\mathrm{sig}}^{\mathrm{tag}}$ is the efficiency and D the dilution. We use a per-candidate analysis that uses both the information of the tag decision and of the predicted mistag probability to classify and assign a weight to each event. The PDFs of the predicted mistag are taken from the side-bands for the background and side-band subtracted data for the signal.

The calibration procedure uses a linear dependence between the estimated per event mistag probability η and the actual mistag probability ω given by $\omega = p_0 + p_1 \cdot (\eta - \langle \eta \rangle)$, where p_0 and p_1 are calibration parameters and $\langle \eta \rangle$ is the average estimated mistag probability as determined from the calibration sample. In the 2011 data $p_0 = 0.384 \pm 0.003 \pm 0.009$, $p_1 = 1.037 \pm 0.040 \pm 0.070$, and $\langle \eta \rangle = 0.379$, with similar values in the 2010 sample. In this paper whenever two errors are given, the first is statistical and the second systematic. Systematic uncertainties are evaluated by using different channels to perform the calibration including $\overline{B}^0 \rightarrow D^{*+} \mu^- \overline{\nu}$, $B^+ \rightarrow J/\psi K^+$ separately from $B^- \rightarrow J/\psi K^-$, and viewing the dependence on different data taking periods. For our 2011 sample $\epsilon_{\mathrm{sig}}^{\mathrm{tag}}$ is $(25.6 \pm 1.3)\%$ providing us with 365 ± 22 tagged signal events. For signal the mean mistag fraction, $\langle \eta \rangle$, is 0.375 ± 0.005, while for background the mean is 0.388 ± 0.006. After subtracting background using like-sign events, we determine $D = 0.289$ leading to an ϵD^2 of 2.1% [14].

6 Results

Several parameters are input as Gaussian constraints in the fit. These include the LHCb measured value of $\Delta m_s = (17.63 \pm 0.11 \pm 0.02)\,\mathrm{ps}^{-1}$ [15], the tagging parameters p_0 and p_1, and both the decay width given by the $J/\psi \phi$ analysis of $\Gamma_s = (0.657 \pm 0.009 \pm 0.008)\,\mathrm{ps}^{-1}$ and $\Delta\Gamma_s = (0.123 \pm 0.029 \pm 0.011)\,\mathrm{ps}^{-1}$ [16]; we also include the correlation of -0.30 between Γ_s and $\Delta\Gamma_s$.[2] The fit has been validated both with samples generated from PDFs and with full Monte Carlo simulations.

Fig. 7 shows the difference of log-likelihood value compared to that at the point with the best fit, as a function of ϕ_s. At each ϕ_s value, the likelihood function is maximized with respect to all other parameters. The best fit value is $\phi_s = -0.44 \pm 0.44\,\mathrm{rad}$. The projected decay time distribution is shown in Fig. 8.

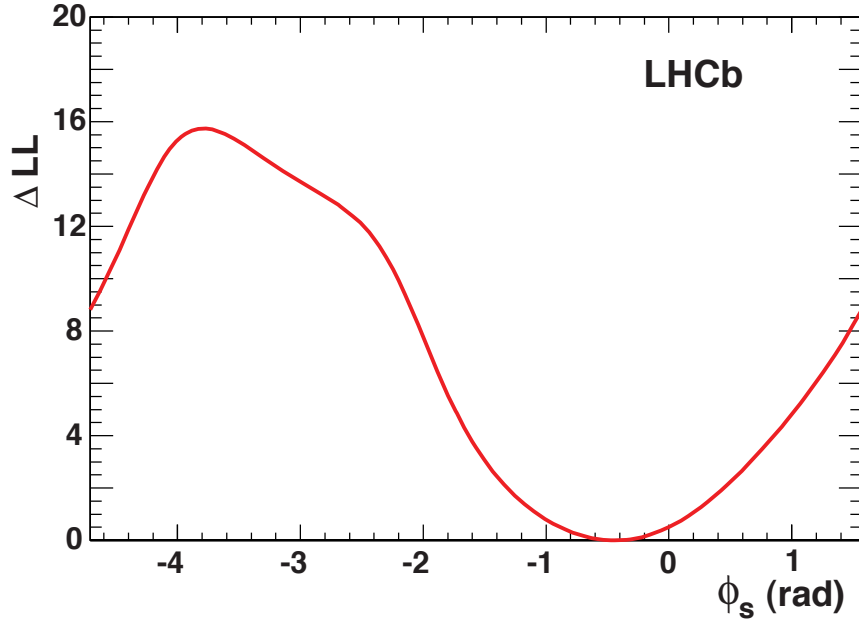[2]The final fitted values of these parameters are shifted by less than 2% from their input values.

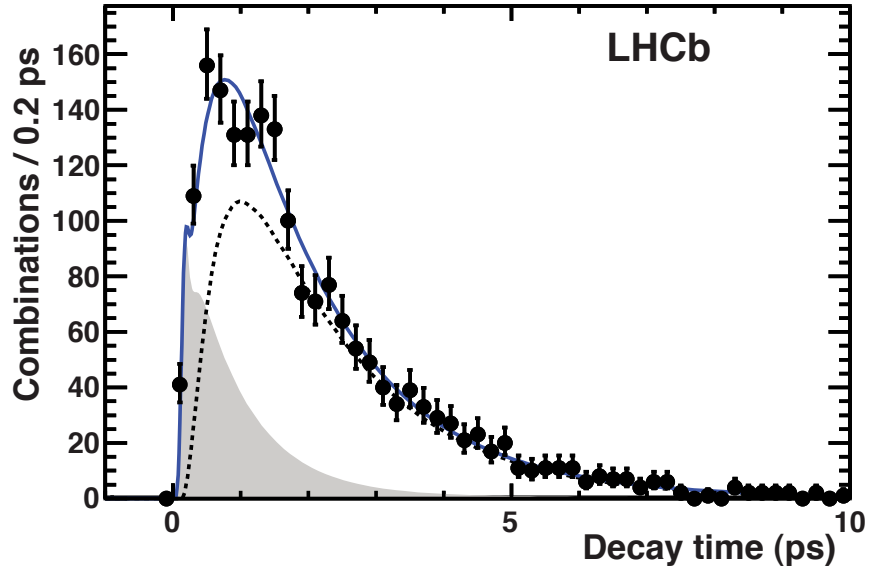Figure 7: Log-likelihood profile of ϕ_s for $\overline{B}_s^0 \to J/\psi f_0$ events.

Figure 8: Decay time distribution from the fit for $J/\psi f_0$ candidates. The solid line shows the results of the fit, the dashed line shows the signal, and the shaded region the background.

7   Systematic uncertainties

The systematic errors are small compared to the statistical errors. No additional uncertainty is needed for errors on Δm_s, Γ_s, $\Delta\Gamma_s$ or flavour tagging, since Gaussian constraints

11

are applied in the fit. Other uncertainties associated parameters fixed in the fit are evaluated by changing them by ± 1 standard deviation from their nominal values and determining the change in fit value of ϕ_s. These are listed in Table 2. An additional uncertainty is included due to the possible CP even D-wave. This has been measured at $(0.0^{+1.7}_{-0.0})\%$ of the S-wave and contributes a small error to ϕ_s, $+0.007$ rad, as determined by repeating the fit with the mistag rate increased by 1.7%. The asymmetry in production between B^0_s and $\overline{B}^0_s$ is believed to be small, about 1%, and similar to the same asymmetry in B^0 production which has been measured by LHCb to be about 1% [17]. The effect of neglecting a 1% production asymmetry is the same as ignoring a 1% difference in the mistag rate and causes negligible bias in ϕ_s.

Table 2: Summary of systematic uncertainties. Here N_{bkg} refers to the number of background events, N_{sig} the number of signal, $N_{\eta'}$ the number of η', α the exponential background parameter for the $\overline{B}^0_s$ candidate mass, $N_{\text{LL}}/N_{\text{bkg}}$ the long-lived background fraction. The Gaussian signal parameters are the mean m_0, the width $\sigma(m)$; t_0, a and n are the three parameters in the acceptance time function. The resolution in signal time is given by $\sigma(t)$, and the background lifetime by τ_{bkg}. The final uncertainty is found by adding all the sources in quadrature.

Quantity (Q)	$\pm \Delta Q$	+Change in ϕ_s	−Change in ϕ_s
N_{bkg}	10.1	0.0025	−0.0030
$N_{\eta'}$	3.4	−0.0001	−0.0001
N_{sig}	46.47	−0.0030	0.0028
α	$1.7 \cdot 10^{-4}$	−0.0002	−0.0002
$N_{\text{LL}}/N_{\text{bkg}}$	0.0238	0.0060	−0.0063
m_0 (MeV)	0.32	-0.0003	0.0011
$\sigma(m)$ (MeV)	0.31	−0.0026	0.0020
τ_{bkg} (ps)	0.05	−0.0075	0.0087
$\sigma(t)$ (ps)	5%	−0.0024	0.0022
t_0 (ps)	0.015	0.0060	0.0050
a (ps^{-1})	0.07	−0.0065	−0.0065
n	0.12	−0.0089	−0.0089
CP-even D-wave		0.0070	0
Total Systematic Error		+0.018	−0.017

8 Conclusions

Using $0.41\,\text{fb}^{-1}$ of data collected with the LHCb detector, the decay mode $\overline{B}^0_s \rightarrow J/\psi f_0$, $f_0 \rightarrow \pi^+\pi^-$ is selected and then used to measure the CP violating phase, ϕ_s. We perform a time dependent fit of the data with the $\overline{B}^0_s$ lifetime and the difference in widths of the

heavy and light eigenstates constrained. Based on the likelihood curve in Fig. 7 we find

$$\phi_s = -0.44 \pm 0.44 \pm 0.02 \text{ rad},$$

consistent with the SM value of $-0.0363^{+0.0016}_{-0.0015}$ rad [1]. Assuming the SM , the probability to observe our measured value is 36%. There is an ambiguous solution with $\phi_s \to \pi - \phi_s$ and $\Delta\Gamma_s \to -\Delta\Gamma_s$. The precision of the result mostly results from using the tagged sample, though the untagged events also contribute.

LHCb provides an independent measurement of $\phi_s = 0.15 \pm 0.18 \pm 0.06$ [16] using the $\bar{B}^0_s \to J/\psi\phi$ decay. Combining these two results, taking into account all correlations by performing a joint fit, we obtain

$$\phi_s = 0.07 \pm 0.17 \pm 0.06 \text{ rad} \quad \text{(combined)}.$$

This is the most accurate determination of ϕ_s to date, and is consistent with the SM prediction.

Acknowledgements

References

[1] J. Charles et al., *Predictions of selected flavour observables within the Standard Model*, *Phys. Rev.* **D84** (2011) 033005, [arXiv:1106.4041].

[2] I. Dunietz, R. Fleischer, and U. Nierste, *In pursuit of new physics with B_s decays*, *Phys. Rev.* **D63** (2001) 114015, [arXiv:hep-ph/0012219].

[3] S. Stone and L. Zhang, *S-waves and the Measurement of CP Violating Phases in B_s Decays*, *Phys. Rev.* **D79** (2009) 074024, [arXiv:0812.2832].

[4] LHCb collaboration, R. Aaij et al., *First observation of $B_s \to J/\psi f_0(980)$ decays*, *Phys. Lett.* **B698** (2011) 115–122, [arXiv:1102.0206].

[5] Belle collaboration, J. Li et al., *Observation of $B_s^0 \to J/\psi f_0(980)$ and Evidence for $B_s^0 \to J/\psi f_0(1370)$*, *Phys. Rev. Lett.* **106** (2011) 121802, [arXiv:1102.2759]; D0 collaboration, V. M. Abazov et al., *Measurement of the relative branching ratio of $B_s^0 \to J/\psi f_0(980)$ to $B_s^0 \to J/\psi\phi$*, arXiv:1110.4272.

[6] CDF collaboration, T. Aaltonen et al., *Measurement of branching ratio and B_s^0 lifetime in the decay $B_s^0 \to J/\psi f_0(980)$ at CDF*, *Phys. Rev.* **D84** (2011) 052012, [arXiv:1106.3682].

[7] S. Faller, R. Fleischer, and T. Mannel, *Precision Physics with $B_s^0 \to J/\psi\phi$ at the LHC: The Quest for New Physics*, *Phys. Rev.* **D79** (2009) 014005, [arXiv:0810.4248]; R. Fleischer, R. Knegjens, and G. Ricciardi, *Anatomy of $B_{s,d}^0 \to J/\psi f_0(980)$*, arXiv:1109.1112.

[8] U. Nierste, *Three Lectures on Meson Mixing and CKM phenomenology*, arXiv:0904.1869; I. I. Bigi and A. Sanda, *CP violation*, *Camb. Monogr. Part. Phys. Nucl. Phys. Cosmol.* **9** (2000) 1–382.

[9] LHCb collaboration, A. Alves Jr. et al., *The LHCb Detector at the LHC*, *JINST* **3** (2008) S08005.

[10] T. Sjostrand, S. Mrenna, and P. Z. Skands, *PYTHIA 6.4 Physics and Manual*, *JHEP* **0605** (2006) 026, [arXiv:hep-ph/0603175].

[11] S. Agostinelli et al., *GEANT4: A Simulation toolkit*, *Nucl. Instrum. Meth.* **A506** (2003) 250–303.

[12] R. Kutsckhe, *An Angular Distribution Cookbook*, *http://home.fnal.gov/∼kutschke/Angdist/angdist.ps* .

[13] Particle Data Group, K. Nakamura et al., *Review of particle physics*, *J. Phys.* **G37** (2010) 075021.

[14] LHCb collaboration, R. Aaij et al., *Flavour tagging of B mesons at LHCb*, LHCb-PAPER-2011-027. In preparation. To be submitted to Eur. J. Phys. C.

[15] LHCb Collaboration, R. Aaij et al., *Measurement of the $B_s^0 - \overline{B}_s^0$ oscillation frequency Δm_s in the decays $B_s^0 \to D_s(3)\pi$*, `arXiv:1112.4311`.

[16] LHCb Collaboration, R. Aaij et al., *Measurement of the CP-violating phase ϕ_s in the decay $B_s^0 \to J/\psi\phi$*, `arXiv:1112.3183`.

[17] LHCb collaboration, *Charmless charged two-body B decays at LHCb with 2011 data*, LHCb-CONF-2011-042.